European Journal of Pharmaceutics and Biopharmaceutics 79 (2011) 328–333

Contents lists available at ScienceDirect

European Journal of Pharmaceutics and Biopharmaceutics

journal homepage: www.elsevier.com/locate/ejpb

Research paper

ToF-SIMS analysis of ocular tissues reveals biochemical differentiation and drug distribution

Jenifer Mains, Clive Wilson, Andrew Urquhart *

Strathclyde Institute of Pharmacy and Biomedical Sciences, University of Strathclyde, Glasgow, Scotland, United Kingdom

ARTICLE INFO

Article history:
Received 17 January 2011
Accepted in revised form 12 April 2011
Available online 21 April 2011

Keywords:
Ocular
Drug
Time-of-flight secondary ion mass spectrometry
Principle component analysis
Multivariate statistics

ABSTRACT

Time-of-flight secondary ion mass spectrometry (ToF-SIMS) was used to obtain mass spectra from three ocular tissues, the lens, the vitreous and the retina. All three tissues were extracted from control ovine eyes and ovine eyes treated with model drug. To identify variations in surface biochemistry of each ocular tissue, principal component analysis (PCA) was applied to ToF-SIMS data. Interesting physiological differences in Na^+ and K^+ distribution were shown across the three tissue types, with other elements including Ca^{2+} and Fe^{2+} distribution also detected. In addition to the identification of small molecules and smaller molecular fragments, larger molecules such as phosphocholine were also detected. The ToF-SIMS data were also used to identify the presence of a model drug compound (amitriptyline – chosen as a generic drug structure) within all three ocular tissues, with model drug detected predominantly across the vitreous tissue samples. This study demonstrates that PCA can be successfully applied to ToF-SIMS data from different ocular tissues and highlights the potential of coupling multivariate statistics with surface analytical techniques to gain a greater understanding of the biochemical composition of tissues and the distribution of pharmaceutically active small molecules within these tissues.

1. Introduction

Time-of-flight secondary ion mass spectrometry (ToF-SIMS) is an extremely surface sensitive spectrometric technique that can provide detailed chemical information of a wide variety of systems, including biological tissue [1,2], drug formulations [3] and polymers [4]. ToF-SIMS has previously been successfully applied to ocular tissues; however, studies have been limited and mainly focused on physiological composition of retina tissue from a specific animal model [5–10]. Work by Amemiya et al. demonstrated the presence of vitamin A and E in cross sections of rat retina as well as differences in counts obtained in response to light stimulus [5]. Using the same model, the group also showed differences in retina expression of fatty acids (maleic, palmitic, oleic, stearic, arachidonic and docosahexaenoic acid) with the highest counts obtained for maleic acid [6]. The ability of ToF-SIMS to spatially map sample cross sections was not exploited in this retinal work as in each case work focussed on total ion counts measured for the whole-tissue cross section. Total ion count is often not an ideal method of direct comparison between samples due to matrix effects where the ion count achieved can vary depending on the chemical environment of the sample [11]. Following on from this work, a study by Kim et al. moved onto demonstrate spatial distribution in ocular tissue by mapping the distribution of Na^+, K^+, Mg^{2+} and Ca^{2+} in the mouse retina [8]. Very limited work has been carried out on lens tissue using the technique of ToF-SIMS with only one study reporting use of this technique. Kinoshita et al. used the rat model to demonstrate that concentration differences of Ca^{2+}, Fe^{2+}, Mg^{2+} and Na^+ existed in 4-month-old rats when compared with 15-month-old rats [12].

Similarly to the lens, limited studies have been performed on the vitreous tissue of the eye. The structure of the vitreous, mainly water, makes it a difficult tissue to prepare and analyse, perhaps explaining the previous lack of use of the ToF-SIMS technique in this tissue. Only one previous study, by Kishikawa et al., has been performed on vitreous tissue, looking at the distribution of various elements, fatty acids and vitamins A and E in patients with diabetic retinopathy and vitreoretinopathy [9]. The vitreous in this case was subjected to a washing stage to facilitate salt removal and was treated as a mass of tissue, analysing the outer layer of the tissue mass rather than a cross section through the tissue. Although ToF-SIMS has been used to consider organic substance distribution within some ocular tissues, ocular tissues have not previously been investigated as a collective to reveal any important physiological differences between tissues. In addition to this, the potential of ToF-SIMS to map drug distribution within ocular tissues has not previously been explored. Interest in mapping drug distribution

* Corresponding author. Strathclyde Institute of Pharmacy and Biomedical Sciences, University of Strathclyde, 161 Cathedral Street, Glasgow, Scotland G4 0RE, United Kingdom. Tel.: +44 0141 548 5947.
E-mail address: andrew.urquhart@strath.ac.uk (A. Urquhart).

0939-6411/$ - see front matter © 2011 Elsevier B.V. All rights reserved.
doi:10.1016/j.ejpb.2011.04.006

within ocular tissues has increased recently, especially when treating certain posterior eye disease states, such as diabetic retinopathy [13] and age-related macular degeneration [14], where effective treatment is currently limited. The process of generating ocular drug distribution data can be time-consuming and requires the eye to be separated into its various ocular tissues. Typically, following separation, ocular tissues are homogenised before the drug is extracted from the tissue, providing no spatial awareness of the drug location within the tissue. The ability to detect drug concentrations directly from a cross section of ocular tissue using ToF-SIMS without the need for extraction method could provide useful distribution information.

Analysis of ToF-SIMS mass spectrum data can be seriously challenging with a simple sample, such as a homopolymer, producing thousands of secondary ion mass peaks [15]. This challenge is increased in magnitude for biological tissue due to the biochemical complexity and composition (from small molecules to kiloDalton weight proteins and polysaccharides) of tissue. It is now commonplace with analytical chemistry to utilise data mining techniques to fully explore large data sets. In the field of ToF-SIMS, both principle component analysis (PCA) [4,16] and partial least squares regression (PLS) [17] are extensively used and have established rules for data pre-processing and processing [16]. PCA is used to establish variance with a data set and determine where the direction of this variance originates. Through the use of PCA, chemically distinct regions in ToF-SIMS data can be identified and key peaks associated with image features selected, in both biological and non-biological samples [18,19]. Prior to carrying out MVA, it is important to select an appropriate means of scaling, as the method selected is widely known to have a major influence on extracting the most useful information from the data set. The use of various data scaling methods has been shown to aid the ability to identify chemical information governing differences within data sets; however, there appears to be no clear guidance on which method is most effective [20]. As a pre-processing step, normalisation is often carried out first before the selected scaling method is applied and PCA carried out. Various types of pre-processing include mean centring, root mean scaling, autoscaling, filter scaling and shift variance scaling. In this study, we show for the first time how PCA can be successfully applied to both positive ToF-SIMS data in order to highlight similarities and differences within the physiological chemistries of the lens, vitreous and retinal ocular tissues. We also present the first use of the ToF-SIMS technique to identify the presence of a model drug compound within these ocular tissues.

2. Materials and methods

2.1. Ocular tissue preparation

A batch of ovine eyes was obtained from a local abattoir within one hour of slaughter. On arrival, the eyes were warmed to body temperature at 37 °C and excess extraorbital tissue and eyelids were removed. Eyes were then cannulated using one of the long ciliary arteries which typically wrap around the optic nerve. A small volume of perfusion fluid was slowly pumped through the eye, whilst the vortex veins were inspected for exit of the perfusion fluid out of eye. Once flow had been established, the eye was introduced into the perfusion system and perfused with physiological media (pH 7.4) based on a method previously used by Koeberle et al. [21]. Eyes were maintained at 37 °C throughout the experiment with a perfusion flow rate of 1 ml/min. Details of the composition of the perfusion fluid administered into the eyes via the ciliary artery are presented in Table 1, all components were purchased from Sigma–Aldrich (Dorset, UK). Once arterial perfusion pressure was maintained, an intravitreal injection of model drug amitriptyline (Fig. 1A) was administered to both eyes. Amitriptyline was identified as a suitable representation of a routinely administered small, generic, biologically active drug molecule. Amitriptyline was selected due to similarities in its basicity, molecular weight and partition coefficient to small drug molecules typically used in the treatment of ocular disease. Intravitreal injections of model drug amitriptyline hydrochloride (Sigma–Aldrich Dorset, UK) were prepared at two concentrations in 100 μl of deionised water. A low dose and a high dose injection were prepared, containing 250 μg and 2000 μg of drug, respectively. The injection was performed using a 1 ml syringe and 23G needle, inserted 1 mm into the vitreous approximately 3–4 mm from the limbus in the posterior direction. Non-perfused eyes, with and without drug administration, were used as controls. To non-perfused eyes with drug administration, intravitreal injection was performed using the same method as perfused eyes. Following exposure for 2 h, the perfusion procedure was ended and perfused eyes were removed from the perfusion kit. All eyes were immediately frozen in liquid nitrogen, and the lens, retina and vitreous were removed. The anterior eye was then cut away in a circular manner and the lens removed. In order to achieve cross sections of the vitreous and the retina, the eye was sliced at four positions from the anterior to the posterior section. The vitreous was removed and the sclera was pressed back for cryosectioning. All tissues were stored at −80 °C prior to sectioning. The lens, vitreous and retina from each eye were mounted onto a cryostat chuck using Shandon M-1 embedding matrix (Thermo-Scientific, Chesire); 20-μm-thick sections were cut through the centre of the tissue on a Leica CM1850 Cryostat (Leica Microsystems, Milton Keynes, UK). Tissue sections were mounted directly onto 1 × 1 cm silicon wafers which were previously cleaned with isopropyl alcohol.

Table 1
Perfusion media composition.

Chemical	Concentration
Tissue culture medium	1000 ml
Sodium bicarbonate	2.2 g/l
Atropine sulphate	0.005 g/l
EDTA	0.2922 g/l
Penicillin G	100k U/l
Streptomycin	75.6kU/l
Gentamycin	0.08 g/l
Insulin bovine	50 U/l
Bovine holo-transferrin	0.0025 g/l
Sodium selenite	2.4 μg/l

2.2. ToF-SIMS analysis

Time-of-flight secondary ion mass spectrometry was performed on an Ion-TOF ToF-SIMS IV instrument (IONTOF, GmbH, Munster, Germany) using a Bi^{3+} cluster source and a single-stage reflectron analyzer. Samples were mounted on a standard sample stage rather than a cold/cryostage as samples were taken directly from frozen conditions and then exposed to ultra high vacuum removing thawing issues. The standard sample stage also allowed greater sample dimension flexibility. A primary ion energy of 25 kV along with a pulsed target current of approximately 1 pA and post-acceleration energy of 10 kV were employed throughout the analysis. The primary ion dose density was maintained at less than 10^{12} ions per cm^2 throughout to ensure static conditions. Spectra were acquired in both positive and negative mode by rastering the stage under the primary ion beam over a sample area of 500 × 500 μm. Low energy electrons (20 eV) were delivered to the sample surface to compensate for positive primary ion beam induced surface charging, a common insulating effect of biological surfaces. Data

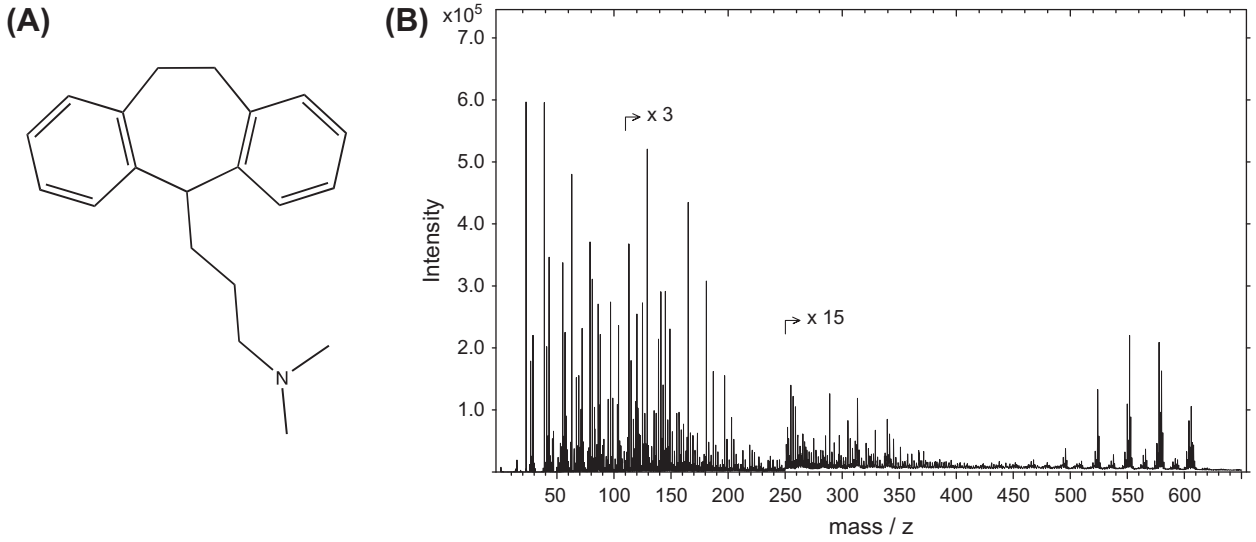

Fig. 1. (A) A schematic showing the structure of amitriptyline. (B) An example of a positive ion spectrum obtained from a vitreous tissue sample.

processing was performed using IonSpec and IonImagesoftware (version 4.0), for spectroscopy and image analysis.

2.3. Multivariate statistics

Statistical analysis was performed using SIMCA-P version 11 (Umetrics, Sweden). Data were exported from IonSpec into Microsoft Excel and divided into three groups; complete sample data, low drug dose data and high drug dose data. The low- and high-dose data sets each contained data for all three tissues from a dosed perfused eye section, a dosed non-perfused eye section and a non-dosed control. Normalisation was carried out as a pre-processing step by dividing total ion count of individual mass peaks obtained for each sample by the total ion count of all peaks calculated for the sample. Following this, mean centring was utilised as an appropriate data scaling method and principle component analysis was performed [29].

3. Results and discussion

In order to analyse lens, retina and vitreous samples by ToF-SIMS, both positive and negative spectra were obtained for all samples. For each of the tissue subtypes and tissue samples, dosed and controls, analysis was performed on three replicates of each sample. Mass spectra obtained for each sample contained numerous peaks with m/z ranging from 1 to 800. Peaks at the lower end of the mass spectra dominated, with greater peak intensities achieved in the m/z range of 1–200 (Fig. 1B). A peak list was generated using a method detailed previously by Urquhart et al. [4]. From the spectra obtained, poor sample separation was observed with the negative ion spectra whereas strong sample separation was shown using the positive ion spectra. It is often the case that with negative spectra, poor sample separation is observed and information obtained using the negative spectrum can often be less specific [4]. The positive ion spectra were used in this study, as they enabled a more interesting and in-depth peak list to be generated and applied to the data. In the positive spectra, 774 ion peaks were selected and added to produce a peak list. After applying the generated peak list to every sample spectrum, the spectra were normalised, before carrying out data processing. To investigate model drug location on the sample surface and identify key model drug peaks, PCA was performed on the positive ion data sets obtained after scaling each of the data sets. It appears that the selection of a suitable pre-processing method can often depend on the individual data set, with only small differences noted when comparing scaling methods, however, is it noted that PCA of scaled data is a vast improvement on PCA of unscaled data [22]. During the data processing step of this work, we explored the use of mean centring, root mean scaling and autoscaling. Mean centring revealed the greatest information from the data and as a result became the focus of this work. Principle components (PC) 1 and 2 demonstrated the best discrimination between tissue subtypes, separating out clearly the lens, retina and vitreous samples, whilst covering 83% of the cumulative variance.

Fig. 2A shows the scores plot obtained for the first two PC's for the positive ion spectra of all tissue samples, and Fig. 2B shows the scores plot obtained for the control samples of each tissue only. From both plots, it is clear that the three ocular tissue subtypes, the lens, retina and vitreous, group together as three distinct groups, reflecting the physiological differences between the tissues. Often in the analysis of biological samples in the first instance, a salt washing step is employed during sample preparation to reduce the salt concentration, as often salts present within the sample surface are associated with the induction of peak suppression [23]. Salt washing has been shown previously to counteract some effects associated with salt suppression; however, the removal effect of the washing phase reduces the secondary ion yield generated which can result in the loss of important biological information [23]. In this work, no salt washing step was utilised as in this case salts were not viewed as contaminations but as biologically important tissue determinants. Good sample clustering was obtained for all three tissue types without the need for a salt washing step (Fig. 2A). The loadings plot of PC 1 and 2 (Fig. 3A) contains the mass peak data used to create the score plot. Suggested structural ion assignments detailing relevant peaks to PC 1 and 2 are detailed in Table 1 and show that salt peaks were important in determining biological differences between tissue types.

Interesting biochemical information and chemical physiological determinants of ocular subtypes were identified. Positive PC 1 values were strongly associated with physiological salts, with m/z = 23 and 39 corresponding to Na^+ and K^+, respectively (Fig. 2A and Table 1). On PC 2 from Fig. 2A, positive PC 2 values were associated with Na^+ (m/z = 23) and negative PC 2 values are associated

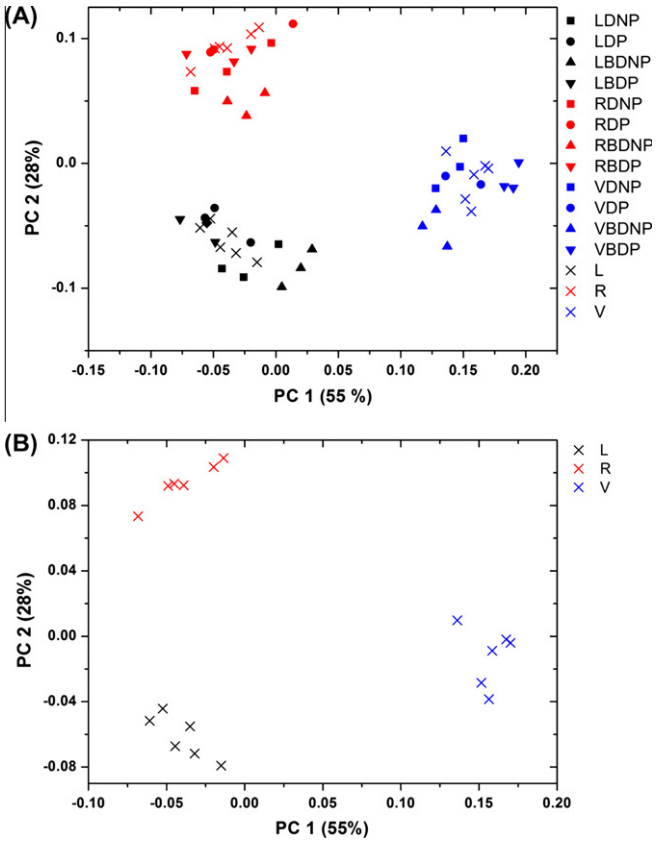

Fig. 2. (A) The scores plot for PC 1 versus PC 2 using positive ion spectra obtained for all ocular tissues samples. L corresponds to lens, V to vitreous and R to retina. DNP corresponds to low dosed non-perfused controls and BDNP to high dosed non-perfused. DP corresponds to low dosed perfused samples and BDP to high dosed perfused samples. (B) The scores plot for PC 1 versus 2 using positive ion spectra obtained control tissue samples. L corresponds to lens, V to vitreous and R to retina.

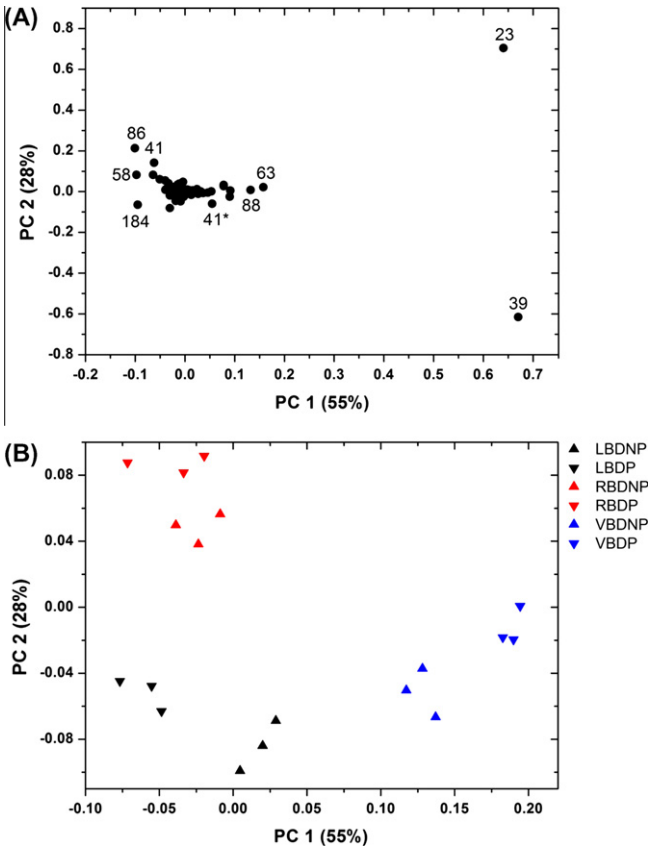

Fig. 3. (A) The loadings plot for PC 1 versus PC 2 demonstrating ion fragments controlling sample discrimination for positive ion spectra. (B) The scores plot for PC 1 versus 2 using positive ion spectra obtained high dosed tissue samples. B represents the scores plot for PC 2 versus 3 using positive ion spectra obtained for all ocular tissues samples. L corresponds to lens, V to vitreous and R to retina. DNP corresponds to low dosed non-perfused controls and BDNP to high dosed non-perfused. DP corresponds to low dosed perfused samples and BDP to high dosed perfused samples.

with K^+ (m/z = 39). The vitreous tissue lies on the positive region of PC 1 demonstrating that this structure is almost completely dominated by Na^+ and K^+ ions. This is in keeping with the known alkali metal composition of the vitreous [24,25]. Other physiological components of the vitreous are likely not to be seen, due to the sheer magnitude of the salt peaks obtained overshadowing any other biochemical peaks obtained. The vitreous tissue has much higher concentrations of Na^+ and K^+ when compared with the lens and the retina, as both of these tissues sit on the negative region of PC 1. The lens and the retina tissues are predominantly separated on PC 2 by differences in Na^+ and K^+ ion concentration. The lens tissue, sits within the negative region of PC 2, demonstrates a high K^+ concentration (m/z = 39) rather than a high Na^+ concentration (m/z = 23). The lens is known to contain Na^+, K^+ and Ca^{2+} with these ions thought to control fluid circulation and nutrient movement [26]. It is extremely interesting that the ovine lens appears to be a richer source of K^+ than Na^+, as previously the human lens has been reported to contain Na^+ concentrations twice that of K^+ [27]. The difference in K^+ prevalence between the human lens and ovine lens represents an interesting species variation in lens tissue electrolyte composition. The retinal tissue sits within the positive region of PC 2, demonstrating that the retina is very different to the lens in the sense that it is dominated by the Na^+ ions rather than the K^+ ions. Differences in Na^+ and K^+ concentrations between the lens and retina have not been previously reported and this shows an interesting difference in ion importance within these tissues.

In addition to Na^+ and K^+, Ca^{2+} ions (m/z = 41) were also detected in the tissue samples; however, two ion peaks of m/z = 41 were obtained, one of which represented Ca^{2+} and the other representing an organic hydrocarbon peak [2]. The first peak at 41 was associated with a positive value on PC 1, whereas the second peak at 41 sat on the negative region of PC 1. On PC 2, positive directionality was associated with the first peak at 41 and negative values associated the second m/z of 41. The retina sat within the negative region of PC 1 and the position region on PC 2, with positioning influenced by the second m/z of 41. The presence of Ca^{2+} in the retina is already well established with the presence of Ca^{2+} in the retina of mice demonstrated previously using ToF-SIMS [8]. Although Ca^{2+} is also present in the lens and vitreous, the Ca^{2+} content in the retina is high [28] due to the essential role of Ca^{2+} in the visual process [29]; therefore, the second peak with m/z 41 in Fig. 2B represented Ca^{2+}. A peak of m/z = 63 was also detected and associated with positive directionality on PC 1 and also positive directionality on PC 2. A positive value on both PC 1 and PC 2 was associated with the vitreous tissue. Copper (m/z = 63, Cu^{2+}) is known to reside in the human vitreous, and the levels are often found to be increased during vitreoretinal diseases such as diabetic retinopathy [30]. The ocular tissues used in this work come from healthy ovine eyes sacrificed at a young age; therefore, it is unlikely the ocular tissues investigated would have increased Cu^{2+} levels. In addition, the positioning of ion m/z = 63 on Fig. 3A shows only a weak pull in the positive direction; therefore, it is likely this peak is commonly found in all three ocular tissues investigated and relates to a typical hydrocarbon species $C_5H_3^+$, commonly seen in positive ion spectra

and likely deriving from phenylalanine, tryptophan and tyrosine, which contain aromatic ring structures [31].

Using ToF-SIMS, we were not only able to detect small molecules, but interestingly we were able to detect smaller fragments of larger molecules found in ocular tissues. Phosphocholine fragments, including the phosphocholine head group $C_5H_{15}NPO_4^+$ with m/z 184, were shown to be present in the ocular tissue samples (Fig. 3A and Table 2). Negative PC 1 values were strongly associated with $C_5H_{15}NPO_4^+$, however, another ocular constituent, vitamin A is also known to fragment and produce ions with a corresponding m/z of 184 [5,32]. The lens tissue sits within the negative regions of PC 1 and 2 and is dominated by the peak at a m/z of 184. The lens is well known to contain vitamin C [33]; however, vitamin A content is of the lens is unclear. On the other hand, the retinal content of vitamin A [5] is well established due to the essential role of vitamin A in the visual process [34]. If the peak at m/z = 184 was induced by a fragment of vitamin A, it would feature on the positive side of PC 2, where the retina samples lie and not where the lens samples sit. The lens is composed of fibre cells, which are surrounded by a phospholipid bilayer and as a result phosphocholine concentrations are likely to be high. Due to the position and importance of mass peak of m/z = 184 in the distribution of the lens samples, m/z of 184 represents $C_5H_{15}NPO_4^+$. In addition to the phospholipid fragment identified, other potential fragments of larger molecules were also detected. A negative pull on PC 1, where the retina samples are positioned, was associated with a mass peak of m/z = 86 and represents either another phosphocholine fragment or the amino acid leucine [35].

In addition to the identification of physiological ocular constituents on PC 1 and PC 2, information about the location of amitriptyline is also evident on these components. Within each of the tissue subtypes, sample grouping of model drug-treated samples and untreated samples is evident. In the vitreous tissue samples, both the high dosed perfused samples and the high dosed non-perfused samples group together. Within the lens and the retina samples, grouping is present within samples treated with a high dose of drug, but only within samples that were dosed and non-perfused (Fig. 3B). The model drug was administered directly into the vitreous of treated eyes that were either perfused or non-perfused. In the non-perfused eye, drug movement through the eye occurred by diffusion alone resulting in drug not being cleared out of the eye due to the lack of blood flow. Therefore, the highest drug concentrations would likely be seen in non-perfused, treated eyes where the total dose remained in the eye and was not cleared. This explains the grouping together of the non-perfused-treated eye samples within the tissue groups for all three ocular tissues. In perfused eye samples, ocular flow systems were enabled, resulting in drug movement through the eye by both diffusion and convection processes, in addition to this, drug clearance from the vortex veins was also in operation [36]. This clearance accounts for the lack of grouping between perfused-treated eye samples of the lens and retina. For the vitreous, the grouping together of perfused-treated samples suggests that a significant drug concentration still remained present within the vitreous. As the vitreous is an avascular structure, movement within the vitreous will often remain slow, even whilst flow systems are in operation within the eye. For this reason, a significant drug concentration remained within the vitreous, explaining the grouping in this tissue. Although the presence of the drug molecule is evident in PC 1 versus PC 2 (Fig. 2A), the biochemical composition of the individual ocular tissue dominates the multivariate analysis and has overshadowed peaks related to the model drug. Two peaks remain undetermined on PC 1 and PC 2, m/z of 58 and m/z of 88, and are possible fragments of the model drug (Fig. 3A). The difficultly in identifying drug peaks could be related to the dose of drug administered to the eye and/or the similarity of the drug structure to organic tissue constituents. However, even with these difficulties, the presence of the drug is evident on PC 1 and PC 2 and is a highly promising result.

This work has demonstrated that PCA can be applied to ToF-SIMS data in order to gain key physiological chemical information of ocular tissues and identify important physiological differences between ocular subtypes. The ability to detect and identify physiological constituents holds significant value in adding to the understanding of the structural components of the lens, vitreous and retinal tissues. PCA has also successfully detected model drug presence within ocular tissues, showing differences between ocular tissues treated with model drug and control ocular tissues. Although challenges arose in identifying specific drug fragments, this preliminary piece of work shows good promise in the use of the ToF-SIMS technique to identify drug location within ocular tissues. However, further work is still required in order to progress the use of ToF-SIMS in identifying drug distribution in ocular tissues. Studies focusing on a drug containing distinct chemical groups not typically seen in the ocular tissues analysed, such as a fluorinated compound, is of interest and would aid the identification of specific drug fragments.

Table 2
Ion fragments (m/z) and structural assignment for positive ion spectra.

m/z	Positive ion structure
22.9930	Na^+
29.0409	$C_2H_5^+$
30.0378	CH_4N^+
38.9687	K^+
40.9660	Ca^+
43.0565	CH_3CO^+
44.0529	$C_2H_6N^+$
55.0568	Fe^+
63.0214	$C_5H_3^+$
70.0728	$C_4H_8N^+$
71.9842	FeO^+
72.0860	$C_5H_{12}N^+$
86.1090	$C_4H_8NO^+$ or $C_5H_{12}N^+$
94.9363	$C_7H_{10}^+$
104.1218	$C_5H_{14}NO^+$
147.0273	$C_2H_5O_4PNa^+$
184.1090	$C_5H_{15}NPO_4^+$

Acknowledgements

JM acknowledges AstraZeneca and University of Strathclyde for the studentship. We thank Dr David Scurr from Laboratory of Biophysics and Surface Analysis (LBSA), School of Pharmacy, University of Nottingham for assistance with ToF-SIMS measurements.

References

[1] K. Börner, H. Nygren, P. Malmberg, E. Tallarek, B. Hagenhoff, Localization of Na^+ and K^+ in rat cerebellum with imaging TOF-SIMS, Applied Surface Science 252 (2006) 6777–6781.
[2] L. Wu, X. Lu, K.S. Kulp, M.G. Knize, E.S.F. Berman, E.J. Nelson, J.S. Felton, K.J.J. Wu, Imaging and differentiation of mouse embryo tissues by ToF-SIMS, International Journal of Mass Spectrometry 260 (2007) 137–145.
[3] A.M. Belu, M.C. Davies, J.M. Newton, N. Patel, TOF-SIMS characterization and imaging of controlled-release drug delivery systems, Analytical Chemistry 72 (2000) 5625–5638.
[4] A.J. Urquhart, M. Taylor, D.G. Anderson, R. Langer, M.C. Davies, M.R. Alexander, TOF-SIMS analysis of a 576 micr patterned copolymer array to reveal surface moieties that control wettability, Analytical Chemistry 80 (2007) 135–142.
[5] T. Amemiya, H. Gong, K. Takaya, M. Tozu, Y. Ohashi, Changes of vitamins A and E in the rat retina under light and dark conditions detected with TOF-SIMS, Applied Surface Science 203–204 (2003) 738–741.
[6] T. Amemiya, M. Tozu, Y. Ohashi, Time-of-flight secondary ion mass spectrometry can replace histochemistry demonstration of fatty acids in the retina, Japanese Journal of Ophthalmology 48 (2004) 287–293.

[7] H. Gong, T. Amemiya, K. Takaya, M. Tozu, Y. Ohashi, Time-of-flight secondary ion mass spectrometry of fatty acids in rat retina, Applied Surface Science 203–204 (2003) 734–737.
[8] J.H. Kim, J.H. Kim, B.J. Ahn, J.H. Park, H.K. Shon, Y.S. Yu, D.W. Moon, T.G. Lee, K.W. Kim, Label-free calcium imagine in ischemic retinal tissue by TOF-SIMS, Biophysical Journal 94 (2008) 4095–4102.
[9] Y. Kishikawa, H. Gong, T. Kitaoka, T. Amemiya, K. Takaya, M. Tozu, T. Hoshi, Y. Ohashi, Elements and organic substances in epiretinal proliferative tissue excised during vitreous surgery: analysis by time-of-flight secondary-ion mass spectrometry, Japanese Society of Microscopy 52 (2003) 349–354.
[10] Y. Kishikawa, T. Suematsu, T. Kitaoka, M. Tozu, T. Hoshi, Y. Ohashi, Analysis of internal limiting membranes of secondary macular hole and idiopathic macular hole by time-of-flight secondary ion mass spectrometer, Investigative Ophthalmology and Visual Science 46 (2005) 5422.
[11] S. Jung, M. Foston, M.C. Sullards, A.J. Ragauskas, Surface characterization of dilute acid pretreated populus deltoides by ToF-SIMS, Energy & Fuels 24 (2010) 1347–1357.
[12] A. Kinoshita, H. Gong, T. Amemiya, K. Takaya, M. Tozu, Y. Ohashi, Trace elements in lenses of normal Wistar Kyoto rats, Applied Surface Science 203–204 (2003) 742–744.
[13] M. Porta, A. Allione, Current approaches and perspectives in the medical treatment of diabetic retinopathy, Pharmacology & Therapeutics 103 (2004) 167–177.
[14] T.Y. Wong, G. Liew, P. Mitchell, Clinical Update: new treatments for age related macular degeneration, The Lancet 370 (2007) 204–206.
[15] M.C. Davies, R.A.P. Lynn, J. Hearn, A.J. Paul, J.C. Vickerman, J.F. Watts, Surface chemical characterization using XPS and TOF-SIMS of latex particles prepared by the emulsion copolymerization of functional monomers with methyl methacrylate and 4-vinyl pyridine, Langmuir 11 (1995) 4313–4322.
[16] J.L.S. Lee, I.S. Gilmore, M.P. Seah, Quantification and methodology issues in multivariate analysis of ToF-SIMS data for mixed organic systems, Surface and Interface Analysis 40 (2008) 1–14.
[17] M. Taylor, A.J. Urquhart, D.G. Anderson, R. Langer, M.C. Davies, M.R. Alexander, Partial least squares regression as a powerful tool for investigating larger combinatorial polymer libraries, Surface and Interface Analysis 41 (2009) 127–135.
[18] B. Tyler, Interpretation of TOF-SIMS images: multivariate and univariate approaches to image de-noising, image segmentation and compound identification, Applied Surface Science 203–204 (2003) 825–831.
[19] M.S. Wagner, D.J. Graham, B.D. Ratner, D.G. Castner, Maximizing information obtained from secondary ion mass spectra of organic thin films using multivariate analysis, Surface Science 570 (2004) 78–97.
[20] M.R. Keenan, P.G. Kotula, Optimal scaling of TOF-SIMS spectrum-images prior to multivariate statistical analysis, Applied Surface Science 231–232 (2004) 240–244.
[21] M.J. Koeberle, P.M. Hughes, G.G. Skellern, C.G. Wilson, Pharmacokinetics and disposition of memantine in the arterially perfused bovine eye, Pharmaceutical Research 23 (2006) 2781–2798.
[22] B.J. Tyler, G. Rayal, D.G. Castner, Multivariate analysis strategies for processing ToF-SIMS images of biomaterials, Biomaterials 28 (2007) 2412–2423.
[23] A.M. Piwowar, N.P. Lockyer, J.C. Vickerman, Salt effects on ion formation in desorption mass spectrometry: an investigation into the role of alkali chlorides on peak suppression in time-of-flight-secondary ion mass spectrometry, Analytical Chemistry 81 (2009) 1040–1048.
[24] E.A. Balazs, J.L. Denlinger, The Vitreous, in: H. Daveson (Ed.), The Eye, Academic Press, 1984, pp. 533–589.
[25] C.S. Nickerson, J. Park, J.A. Kornfield, H. Karageozian, Rheological properties of the vitreous and the role of hyaluronic acid, Journal of Biomechanics 41 (2008) 1840–1846.
[26] D.C. Beebe, Lens, in: P.L. Kaufman, A. Alm (Eds.), Adler's Physiology of the Eye, Mosby Inc., St Louis, Missouri, 2003, pp. 117–158.
[27] N. Dilsiz, A. Olcucu, M. Atas, Determination of calcium, sodium, potassium and magnesium concentrations in human senile cataractous lenses, Cell Biochemistry and Function 18 (2000) 259–262.
[28] H.H. Hess, The high calcium content of retinal pigmented epithelium, Experimental Eye Research 21 (1975) 471–479.
[29] A. Akopian, P. Witkovsky, Calcium and retinal function, Molecular Neurobiology 25 (2002) 113–132.
[30] N.S. Konerirajapuram, K. Coral, R. Punitham, T. Sharma, N. Kasinathan, R. Sivaramakrishnan, Trace elements iron, copper and zinc in the vitreous of patients with various vitreoretinal diseases, Indian Journal of Ophthalmology 52 (2004) 145–148.
[31] H. Zhou, C.M. Chan, L.T. Weng, K.M. Ng, L. Li, Relationship between the structure of polymers with well-defined fluorocarbon segmental lengths and the formation of secondary ions in SIMS, Surface and Interface Analysis 33 (2002) 932–939.
[32] E. Gazi, J. Dwyer, N. Lockyer, P. Gardner, J.C. Vickerman, J. Miyan, C.A. Hart, M. Brown, J.H. Shanks, N. Clarke, The combined application of FTIR microspectroscopy and ToF-SIMS imaging in the study of prostate cancer, Faraday Discussions 126 (2003) 41–59.
[33] E.R. Berman, Biochemistry of the Eye, Plenum Press, New York, 1991.
[34] L. Quadro, W.S. Blaner, D.J. Salchow, S. Vogel, R. Piantedosi, P. Gouras, S. Freeman, M.P. Cosma, V. Colantuoni, M.E. Gottesman, Impaired retinal function and vitamin A availability in mice lacking retinol-binding protein, EMBO Journal 18 (1999) 4633–4644.
[35] M. Aranyosiova, M. Michalka, M. Kopani, B. Rychly, J. Jakubovsky, D. Velic, Microscopy and chemical imaging of Behcet brain tissue, Applied Surface Science 255 (2008) 1584–1587.
[36] S. Tsuboi, J.E. Pederson, Volume flow across the isolated retinal pigmented epithelium of cynomolgus monkey eyes, Investigative Ophthalmology and Visual Science 29 (1988) 1652–1656.